Robust Nonequilibrium Edge Currents with and without Band Topology

Mark T. Mitchison,[1,*] Ángel Rivas,[2,3,†] and Miguel A. Martin-Delgado[2,3,‡]
[1]School of Physics, Trinity College Dublin, College Green, Dublin 2, D02 K8N4, Ireland
[2]Departamento de Física Teórica, Facultad de Ciencias Físicas, Universidad Complutense, 28040 Madrid, Spain
[3]CCS-Center for Computational Simulation, Campus de Montegancedo UPM, 28660 Boadilla del Monte, Madrid, Spain

(Received 21 June 2021; accepted 3 March 2022; published 25 March 2022)

We study two-dimensional bosonic and fermionic lattice systems under nonequilibrium conditions corresponding to a sharp gradient of temperature imposed by two thermal baths. In particular, we consider a lattice model with broken time-reversal symmetry that exhibits both topologically trivial and nontrivial phases. Using a nonperturbative Green function approach, we characterize the nonequilibrium current distribution in different parameter regimes. For both bosonic and fermionic systems, we find chiral edge currents that are robust against coupling to reservoirs and to the presence of defects on the boundary or in the bulk. This robustness not only originates from topological effects at zero temperature but, remarkably, also persists as a result of dissipative symmetries in regimes where band topology plays no role. Chirality of the edge currents implies that energy locally flows against the temperature gradient without any external work input. In the fermionic case, there is also a regime with topologically protected boundary currents, which nonetheless do not circulate around all system edges.

DOI: 10.1103/PhysRevLett.128.120403

Introduction.—The physics of boundary structures, whether they be dots, lines, or surfaces, has attracted a great deal of attention from various directions in the past. The theoretical discovery, and its subsequent experimental verification, of both insulating and superconducting topological materials [1–6] has further spurred the study of boundary physics. The main reason for this is that nontrivial band topology endows edge phenomena with a remarkable robustness. This feature opens up a myriad of possible applications that go well beyond condensed matter physics. Historically, most of the mainstream studies conducted on those topological materials shared two basic properties in common: (i) the quantum system is considered as closed and thus isolated from the detrimental effects of the surrounding environment; (ii) the constituent particles are fermions. The combination of these two properties underpins the stability of boundary effects in topological phases of matter.

In this work, we present a different paradigm of robust boundary physics in which we depart from these two common features, entering less well-trodden ground. The motivation is to study more demanding scenarios corresponding to a quantum system coupled to thermal baths, which generate external noise yielding fluctuations and dissipation [7–11]. In fact, understanding noisy circumstances like these is crucial for the successful development of scalable quantum technologies. In this context, we find that robust edge currents can be generated without resorting to the standard band topological mechanism, focusing our attention not only on fermionic systems, but on bosonic particles as well.

To illustrate this unusual form of dissipative robustness, we consider a bosonic variant of the model previously introduced by Qi, Wu, and Zhang (QWZ) for fermions on a square two-dimensional (2D) lattice [12]. This model has the virtue of presenting two topologically different band structures depending on the values of its coupling parameters. In the fermionic case at half filling, these two correspond to different phases: one is a trivial insulator, and the other a topological insulator. Of course, the single-particle band structure of the QWZ model is the same for fermions and bosons. However, the statistics of the particles determine how those bands are filled. The Pauli principle forces fermions to fill the bands up to the Fermi level, thereby unveiling the band topology. On the contrary, bosons at low temperatures tend to condense in the single-particle ground state, making them largely insensitive to the global band structure.

Remarkably, for both bosonic and fermionic QWZ lattices, we find dissipatively robust, chiral edge currents flowing between two thermal reservoirs in a parameter regime leading to trivial band topology. Here, robustness is defined by stability of the currents with respect to the introduction of defects on the edges or in the bulk. This stability is not arbitrary, but is subject to the fulfilment of discrete symmetries on the geometrical distribution of the defects, which must be compatible with the underlying symmetries of the nonequilibrium steady state (NESS). In the fermionic case, and when the temperature of one of the two reservoirs is much smaller than the band gap, we also observe topologically protected edge currents that are effectively independent of the defect distribution but

may not circulate around every edge of the perturbed system.

The interplay between topology and symmetries in dissipative quantum systems has recently been explored within a Markovian approximation [13–26], which generally requires weak system-reservoir interactions (see also Ref. [27] for non-Markovian extensions in fermionic systems). Here, we instead adopt a nonperturbative Green's function method to compute the exact NESS for arbitrary values of the system-bath coupling, in order to monitor how the current distribution within the system changes from strong to weak coupling regimes. Interestingly, edge currents appear in the weak-coupling limit but are masked by bulk currents at strong coupling. This contrasts with the common expectation that exotic thermodynamic effects are more prone to arise in strong-coupling configurations [28–39]. Our exact analysis can also help to identify the range of parameters in which these dissipative edge currents can be experimentally realized. An appropriate way to achieve such realizations is a setup with a high degree of control over microscopic degrees of freedom, e.g., quantum simulation on platforms developed to deal with large systems [40–51], whose fundamental constituents may be bosons.

How can dissipatively robust edge currents arise without band topology? Let us first explore this phenomenon and then we will explain its origin.

Model.—We consider the QWZ Hamiltonian [12] describing a collection of noninteracting fermions or bosons with two internal "flavor" states. The particles occupy a 2D square lattice with sites specified by the coordinates $x = 1, \ldots, L_X$ and $y = 1, \ldots, L_Y$. The Hamiltonian is expressed in terms of vectors of canonical ladder operators $\hat{\mathbf{a}}^\dagger_{x,y} = (\hat{a}^\dagger_{x,y,\uparrow}, \hat{a}^\dagger_{x,y,\downarrow})$ for each lattice site, whose components create a particle with flavor $\uparrow$ or $\downarrow$. Note that the flavors merely index distinct bands and are unrelated to angular momentum. Explicitly, the Hamiltonian reads as $\hat{H} = \hat{H}_m + \hat{H}_X + \hat{H}_Y$, with ($\hbar = 1 = k_B$)

$$\hat{H}_m = \sum_{x,y} \hat{\mathbf{a}}^\dagger_{x,y} \cdot (\omega_0 \mathbb{1} + m\sigma_z) \cdot \hat{\mathbf{a}}_{x,y}, \tag{1}$$

$$\hat{H}_X = \frac{t_X}{2} \sum_{x,y} \hat{\mathbf{a}}^\dagger_{x+1,y} \cdot (\sigma_z + \mathrm{i}\sigma_y) \cdot \hat{\mathbf{a}}_{x,y} + \mathrm{H.c.}, \tag{2}$$

$$\hat{H}_Y = \frac{t_Y}{2} \sum_{x,y} \hat{\mathbf{a}}^\dagger_{x,y+1} \cdot (\sigma_z + \mathrm{i}\sigma_x) \cdot \hat{\mathbf{a}}_{x,y} + \mathrm{H.c.}, \tag{3}$$

where $\sigma_{x,y,z}$ are Pauli matrices in flavor space, ω_0 is the on-site energy, m is the flavor energy splitting, and $t_{X,Y} > 0$ are the tunneling amplitudes in the x and y directions.

The QWZ Hamiltonian has two notable symmetries. The first is $\hat{\Pi}\hat{R}_\pi$, a combined π rotation about the z axis in real space, $\hat{R}_\pi \hat{\mathbf{a}}_{x,y} \hat{R}^\dagger_\pi = \hat{\mathbf{a}}_{L_X+1-x,L_Y+1-y}$, and flavor space, $\hat{\Pi}\hat{\mathbf{a}}_{x,y}\hat{\Pi}^\dagger = \sigma_z \hat{\mathbf{a}}_{x,y}$. The second symmetry is $\hat{\Pi}\,\hat{\Theta}\,\hat{\Sigma}_y$, which combines time reversal, $\hat{\Theta}\,\hat{H}\,\hat{\Theta}^{-1} = \hat{H}^*$, spatial reflection about the y axis, $\hat{\Sigma}_y \hat{\mathbf{a}}_{x,y} \hat{\Sigma}^\dagger_y = \hat{\mathbf{a}}_{L_X+1-x,y}$, and the flavor π-rotation $\hat{\Pi}$ defined above. We can already anticipate that these discrete symmetries will play an important role in stabilizing edge currents out of equilibrium, as previously found in the context of a bosonic Hofstadter model [19]. Unlike that model, however, the QWZ Hamiltonian exhibits both topologically trivial and nontrivial phases depending on the value of m relative to $t_{X,Y}$. Nontrivial topology manifests as a series of edge states with linear dispersion relation connecting the two single-particle energy bands. Conversely, in the topologically trivial regime there are no edge states and the bands are separated by a finite energy gap. The phase diagram and corresponding band structure is indicated in Fig. 1.

To study an out-of-equilibrium situation, we couple one side of the lattice ($x = 1$) to a hot thermal bath at temperature $T_h = \beta_h^{-1}$ and the other side ($x = L_X$) to a cold bath at temperature $T_c = \beta_c^{-1}$, as depicted in Fig. 1(b). These baths are modeled by reservoirs of noninteracting fermions or bosons, which can tunnel to and from the system via a linear coupling. We assume that reservoir modes coupled to distinct sites of the system are uncorrelated, and are initially populated according to the distribution function $\bar{n}_{h,c}(\omega) = (e^{\beta_{h,c}(\omega-\mu)} \pm 1)^{-1}$, where the plus (minus) sign pertains to fermions (bosons). In the fermionic case, we include a chemical potential μ to fix the average density, while in the bosonic case we set $\mu = 0$. At long times, the system reaches a NESS, which can be computed exactly [52]. The NESS is a Gaussian state and thus fully characterized by its correlation matrix $C_{jk} = \langle \hat{a}^\dagger_k \hat{a}_j \rangle$, where the indices j, k represent the coordinates (x, y) as well as the flavor state. Explicitly, we have

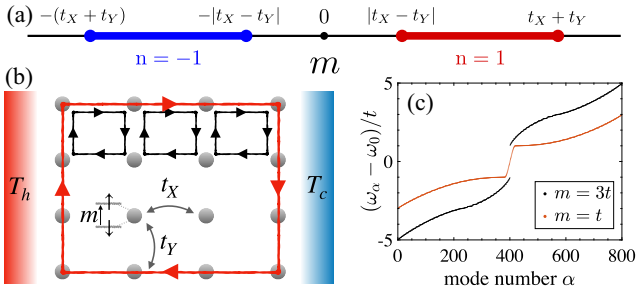

FIG. 1. The QWZ model. (a) Phase diagram showing the topologically nontrivial regimes with nonzero Chern number $n = \pm 1$, a topological invariant of the band structure under periodic boundary conditions [6]. (b) Schematic of the system, featuring a 2D lattice hosting particles with two internal states, coupled to thermal baths at different temperatures. An edge current (red) emerges from an erasure effect where modes with the same current circulation (black) cancel in the bulk but add constructively on the boundary. (c) Single-particle eigenenergies ω_α as a function of the mode index α for a system with open boundary conditions, with $L_X = L_Y = 20$, $t_X = t_Y = t$.

$$\mathbf{C} = \int \frac{d\omega}{2\pi} \mathbf{G}(\omega) \cdot [\mathbf{\Gamma}_h \bar{n}_h(\omega) + \mathbf{\Gamma}_c \bar{n}_c(\omega)] \cdot \mathbf{G}^\dagger(\omega), \quad (4)$$

where $\mathbf{G}(\omega)$ is the retarded Green's function of the system obtained by tracing over the reservoirs and $\mathbf{\Gamma}_{c,h}$ are self-energies describing the system-reservoir coupling [57,58]. We work in the wide-band limit, where the self-energies can be approximated by a frequency-independent constant γ, which we assume to be equal for both hot and cold reservoirs. This approximation, which is valid so long as the reservoir spectral densities vary slowly in the relevant frequency range, significantly simplifies the calculations but is not essential for our conclusions to hold.

The applied thermal gradient gives rise to particle currents flowing within the system. We denote by $J^X_{x,y}$ the mean particle current flowing from site (x, y) to site $(x+1, y)$, while $J^Y_{x,y}$ denotes the current flowing from (x, y) to $(x, y+1)$. These are expectation values of one-body observables and can be found from the NESS correlation matrix $\mathbf{C}$ [52].

Results.—In the following examples, we focus on the symmetric case with $L_X = L_Y = L$ and $t_X = t_Y = t$, so that $|m| < 2t$ defines the topologically nontrivial phase. We also fix $\omega_0 = 10t$ and consider relatively low temperatures, $T_{c,h} \lesssim t$, to accentuate the role of band topology and particle exchange statistics.

Figures 2(a) and 2(b) plot the nonequilibrium current distributions for two different values of the system-reservoir coupling, γ. Red arrows show the currents for a bosonic system with $m = 3t$ (similar results are obtained for $|m| < 2t$). Remarkably, the currents become progressively localized on the boundary of the system as γ is reduced, even though the band topology is trivial. These edge currents also arise in the equilibrium case, $T_h = T_c$, as shown in Fig. 2(c). Qualitatively similar results are obtained for fermions, as shown for a nontrivial phase ($m = t$) by the blue arrows in Fig. 2. The direction of fermionic particle flow depends on the chemical potential; for the parameters in Figs. 2(a) and 2(b), the thermoelectric induced current flows in the opposite direction to the temperature gradient. Conversely, when $\mu = \omega_0$, all currents vanish due to particle-hole symmetry [52].

In order to quantify the emergence of boundary currents more precisely, we define the average edge and bulk currents

$$J_{\text{edge}} = \frac{1}{2L_X} \sum_x (J^X_{x,L_Y} - J^X_{x,1}), \quad J_{\text{bulk}} = \frac{1}{L_Y} \sum_y J^X_{x,y}. \quad (5)$$

The choice of x coordinate in the definition of J_{bulk} is arbitrary due to particle-number conservation; we take $x = \lfloor L_X/2 \rfloor$. The total current flowing between the two reservoirs is given by $J_{\text{tot}} = L_Y J_{\text{bulk}}$.

We plot the edge and bulk currents in Fig. 3 for bosonic and fermionic systems as a function of the system-reservoir coupling strength, γ. In the bosonic case, both bulk and edge currents increase with m and are thus larger in the topologically trivial phase. The situation is reversed for fermions, with the largest edge currents obtained in the topologically nontrivial phase. In all cases, the bulk currents are proportional to γ and thus vanish as $\gamma \to 0$, while the edge currents remain invariant for a wide range of values of γ and persist in the weak-coupling limit. These quantitative results therefore confirm the qualitative picture of Fig. 2, i.e., edge currents arise for small coupling irrespectively of band topology or particle statistics. In topologically trivial phases, edge currents begin to dominate once γ becomes comparable to the level spacing of the single-particle Hamiltonian. However, in the topologically nontrivial phase for fermions near half filling, currents remain localized on the edges even for strong coupling, $\gamma \sim t$.

Finally, we investigate whether these effects withstand the presence of imperfections, a property which defines the

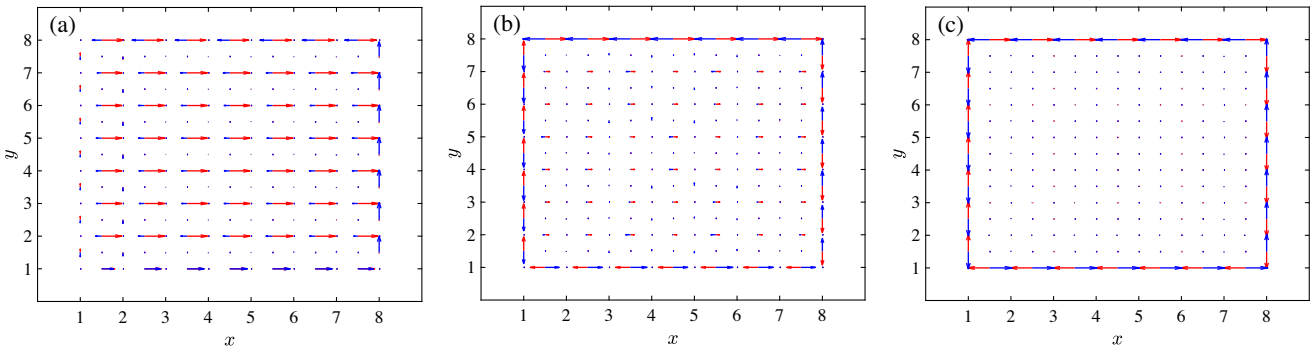

FIG. 2. Current distributions on a lattice of size $L = 8$. Red arrows show boson currents in a topologically trivial phase ($m = 3t$), blue arrows show fermion currents in a topologically nontrivial regime ($m = t$). Arrow sizes indicate the magnitude of the currents scaled relative to the largest value within each plot. (a),(b) Nonequilibrium current profile with different temperatures $T_h = t$ and $T_c = 0.01t$, on-site energy $\omega_0 = 10t$, chemical potential $\mu = \omega_0 - 0.01t$ for fermions (we always set $\mu = 0$ for bosons), and coupling strength (a) $\gamma = 0.5t$ and (b) $\gamma = 0.005t$. (c) Equilibrium case with temperatures $T_c = T_h = t$, weak coupling, $\gamma = 0.005t$, and other parameters identical to (a),(b).

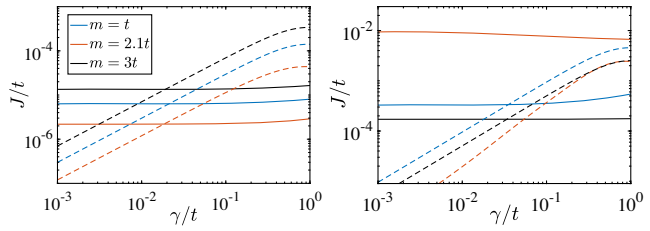

FIG. 3. Average edge currents, J_{edge} (solid lines), and bulk currents, J_{bulk} (dashed lines), as a function of the system-bath coupling strength, γ, for bosons (left panel) and fermions (right panel) in topologically nontrivial ($m/t = 1$) and trivial ($m/t = 2.1, 3$) regimes, and with $T_h = t$, $T_c = 0.01t$, $\omega_0 = 10t$, and $\mu = \omega_0 + 0.1t$.

notion of dissipatively robust currents. Specifically, we examine how the currents change when static impurities are added to the lattice. Impurities are modeled by a large on-site energy shift, i.e., a term $\Delta \hat{\mathbf{a}}^{\dagger}_{x,y} \cdot \hat{\mathbf{a}}_{x,y}$ added to the Hamitonian, where $\Delta \gg \omega_0, t$ and (x, y) are the coordinates of the impurity site [19]. We focus hereafter on the weak-coupling limit where the edge currents are most prominent in the absence of impurities. In this limit, an analytical expression for the NESS [57] can be obtained, which is identical to the solution of the Lindblad equation derived under the Born-Markov and secular approximations [52].

In Fig. 4 we show three examples of how impurities affect the nonequilibrium current distribution in the topologically nontrivial phase. We observe substantial differences between bosonic and fermionic systems when one of the reservoirs is at low temperature. The bosonic edge currents are preserved only when the impurity distribution is invariant under one of the symmetries $\hat{\Pi}\hat{\Theta}\hat{\Sigma}_y$ or $\hat{\Pi}\hat{R}_{\pi}$, which correspond to the purely spatial symmetries $\hat{\Sigma}_y$ and $\hat{R}_{\pi}$ since the defects satisfy $\hat{\Pi}$ and $\hat{\Theta}$ automatically. In the case of impurities placed on the edge (and assuming the symmetries are respected in the bosonic case), the currents simply detour around the impurity sites [Fig. 4(a)]. If impurities are placed in the bulk of a bosonic system in an appropriately symmetric way, countercurrents shield the impurity sites by circulating in the opposite direction to the edge currents [Fig. 4(b)]. In the absence of these symmetries, the bosonic edge currents are strongly disrupted [Fig. 4(c)]. For fermions in a topological phase, the situation is starkly different when at least one reservoir is at low temperature: impurities placed in the bulk have no effect whatsoever on the current distribution [Figs. 4(b) and 4(c)]. In the topologically trivial phase or at high temperature, both bosonic and fermionic edge currents enjoy the same symmetry-protected robustness as bosons in the nontrivial phase.

Discussion.—The question posed in the Introduction on the nontopological origin of the edge currents can now be answered. In the weak-coupling limit, nonequilibrium coherences between energy eigenstates become small [57] and J_{bulk}, which is directly proportional to these coherences [59], is negligible in comparison to the contributions from individual energy eigenstates. Moreover, the single-particle eigenmodes in the QWZ model present a nonzero Berry curvature $\boldsymbol{\mathcal{F}}_{\alpha}$ for $m \neq 0$ [12], which breaks time-reversal symmetry and endows the eigenmodes with a particular chirality. This can be understood in a semiclassical picture [60], where a wave packet propagates with velocity $\mathbf{v}_{\alpha} = \partial_{\mathbf{k}}\omega_{\alpha} + \nabla V \times \boldsymbol{\mathcal{F}}_{\alpha}$, with $\mathbf{k}$ the wave vector and $V(x, y)$ a confining potential describing the edge of the system [61]. Assuming that the nonequilibrium distribution function only depends on energy, the net current due to the derivative term $\partial_{\mathbf{k}}\omega_{\alpha}$ can be shown to vanish in the bulk due to cancellations between positive and negative wave vectors [52]. However, the contribution of the axial force $\nabla V \times \boldsymbol{\mathcal{F}}_{\alpha}$ is nonzero near the boundary, thus generating a net chiral edge current [52]. This erasure effect arises whenever there is broken time-reversal symmetry and a smooth, energetically monotonic distribution of chiral eigenmodes [19]; it is thus independent of exchange statistics or band topology. Intuitively, the effect can be understood in terms of circulating currents that cancel in the bulk but add constructively on the boundary [Fig. 1(b)].

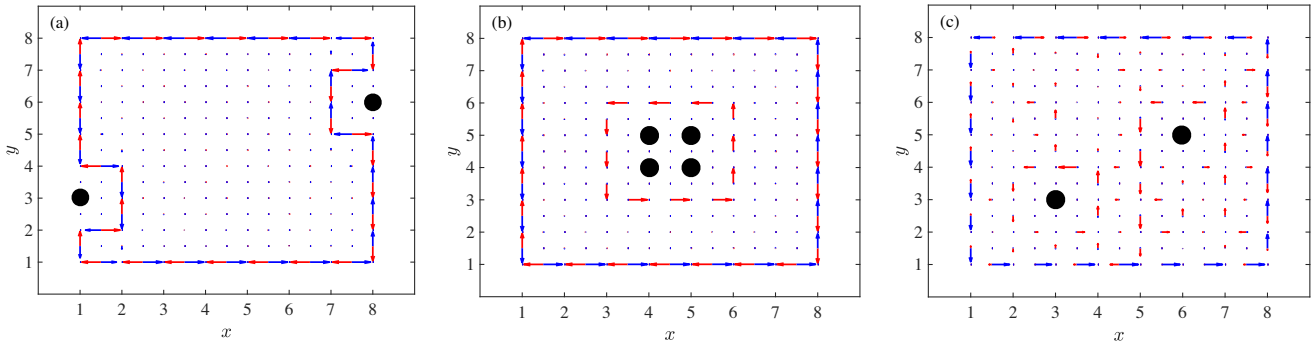

FIG. 4. Effect of impurities on the current distribution in the weak-coupling limit, with impurity positions marked by filled black circles. Red arrows show boson currents and blue arrows show fermion currents. In all plots, $m = t$, $T_h = t$, $T_c = 0.01t$, $\omega_0 = 10t$, and $\mu = \omega_0 - 0.1t$.

A chiral current between two thermal reservoirs unavoidably entails a local cross-current phenomenon: on one edge there are particles flowing from the cold bath to the hot bath. In bosonic systems, this implies a "violation" of the second law of thermodynamics within a one-dimensional subsystem, i.e., energy flows against the temperature gradient along one edge even though the total rate of entropy production is positive. This effect was reported in Refs. [19,62] for bosonic lattices governed by the Hofstadter Hamiltonian. Now, we see that the key requisite for this behavior is not the nontrivial band topology of the lattice, but rather the nonzero Berry curvature in a regime of weak system-bath coupling [Figs. 2(b) and 2(c)].

The edge currents are robust to impurities if the defect distribution satisfies either of the symmetries $\hat{\Pi}\hat{\Theta}\hat{\Sigma}_y$ or $\hat{\Pi}\hat{R}_\pi$. Note that the relevant nonequilibrium symmetries are determined both by the Hamiltonian and by the configuration of the baths. These symmetries leave the NESS invariant and lead to a steady-state correlation matrix that is independent of the spatial orientation of the reservoirs. Under these conditions, the nonequilibrium distribution function is simply the average of the reservoir distributions [52], i.e., $n(\omega_\alpha) = \frac{1}{2}[\bar{n}_h(\omega_\alpha) + \bar{n}_c(\omega_\alpha)]$ is the population of the eigenmode with frequency ω_α. This smooth distribution function yields boundary currents due to the erasure effect in the bulk. In the absence of symmetry, however, the contribution of each mode depends not only on energy but also on the spatial profile of the corresponding wave function. This creates an erratically varying distribution function that destroys the erasure effect [52].

For fermions at low temperature T_c, $n(\omega_\alpha)$ undergoes a sharp change near $\omega_\alpha \approx \mu$. In a topologically nontrivial phase near half filling, this feature acts as a filter that populates only one or two edge states [52], which are topologically protected against perturbations in the bulk. The corresponding boundary current is thus completely unaffected by impurities [Figs. 4(b) and 4(c)]. Remarkably, this holds for arbitrarily large T_h, providing an instance of a topologically protected property that is also stable under dissipation. The number and character of edge modes that contribute to the current pattern is determined by the chemical potential [52].

In summary, our nonperturbative analysis has shown that robust boundary currents emerge at weak coupling in the QWZ lattice driven out of equilibrium by a thermal gradient. Our results reveal a novel dissipative mechanism for symmetry-protected edge transport, which arises in bosonic and fermionic systems with and without nontrivial band topology. This makes quantum simulators based on either fermionic or bosonic degrees of freedom attractive candidates to observe this exotic boundary physics.

M. T. M. acknowledges funding from the ERC Starting Grant ODYSSEY (Grant Agreement No. 758403) and the EPSRC-SFI Joint Funding of Research project QuamNESS. A. R. and M. A. M. D. acknowledges financial support from the Spanish MINECO grants MINECO/FEDER Projects FIS2017-91460-EXP, PGC2018-099169-B-I00 FIS-2018 and from CAM/FEDER Project No. S2018/TCS-4342 (QUITEMAD-CM). The research of A. R. and M. A. M. D. has been partially supported by the U.S. Army Research Office through Grant No. W911NF-14-1-0103. Calculations were performed on the Lonsdale cluster maintained by the Trinity Centre for High Performance Computing. This cluster was funded through grants from SFI.

*mark.mitchison@tcd.ie
†anrivas@ucm.es
‡mardel@ucm.es

[1] F. D. M. Haldane, Phys. Rev. Lett. **61**, 2015 (1988).
[2] C. L. Kane and E. J. Mele, Phys. Rev. Lett. **95**, 226801 (2005).
[3] B. A. Bernevig, T. L. Hughes, and S.-C. Zhang, Science **314**, 1757 (2006).
[4] M. König, S. Wiedmann, C. Brüne, A. Roth, H. Buhmann, L. W. Molenkamp, X.-L. Qi, and S.-C. Zhang, Science **318**, 766 (2007).
[5] X.-L. Qi and S.-C. Zhang, Rev. Mod. Phys. **83**, 1057 (2011).
[6] M. Z. Hasan and C. L. Kane, Rev. Mod. Phys. **82**, 3045 (2010).
[7] H.-P. Breuer and F. Petruccione, *The Theory of Open Quantum Systems* (Oxford University Press, Oxford, 2002).
[8] C. Gardiner and P. Zoller, *Quantum Noise: A Handbook of Markovian and Non-Markovian Quantum Stochastic Methods with Applications to Quantum Optics* (Springer, Berlin, 2004).
[9] A. Kamenev, *Field Theory of Non-Equilibrium Systems* (Cambridge University Press, Cambridge, England, 2009).
[10] A. Rivas and S. F. Huelga, *Open Quantum Systems. An Introduction* (Springer, Heidelberg, 2012).
[11] G. T. Landi, D. Poletti, and G. Schaller, arXiv:2104.14350.
[12] X.-L. Qi, Y.-S. Wu, and S.-C. Zhang, Phys. Rev. B **74**, 085308 (2006).
[13] S. Diehl, E. Rico, M. A. Baranov, and P. Zoller, Nat. Phys. **7**, 971 (2011).
[14] O. Viyuela, A. Rivas, and M. A. Martin-Delgado, Phys. Rev. B **86**, 155140 (2012).
[15] A. Rivas, O. Viyuela, and M. A. Martin-Delgado, Phys. Rev. B **88**, 155141 (2013).
[16] J. C. Budich, P. Zoller, and S. Diehl, Phys. Rev. A **91**, 042117 (2015).
[17] F. Iemini, D. Rossini, R. Fazio, S. Diehl, and L. Mazza, Phys. Rev. B **93**, 115113 (2016).
[18] D. Linzner, L. Wawer, F. Grusdt, and M. Fleischhauer, Phys. Rev. B **94**, 201105(R) (2016).
[19] Á. Rivas and M. A. Martin-Delgado, Sci. Rep. **7**, 6350 (2017).
[20] K. Kawabata, K. Shiozaki, M. Ueda, and M. Sato, Phys. Rev. X **9**, 041015 (2019).
[21] F. Song, S. Yao, and Z. Wang, Phys. Rev. Lett. **123**, 170401 (2019).

[22] G. Shavit and M. Goldstein, Phys. Rev. B **101**, 125412 (2020).
[23] M. Gau, R. Egger, A. Zazunov, and Y. Gefen, Phys. Rev. Lett. **125**, 147701 (2020).
[24] S. Lieu, M. McGinley, and N. R. Cooper, Phys. Rev. Lett. **124**, 040401 (2020).
[25] M. McGinley and N. R. Cooper, Nat. Phys. **16**, 1181 (2020).
[26] V. P. Flynn, E. Cobanera, and L. Viola, Phys. Rev. Lett. **127**, 245701 (2021).
[27] A. Altland, M. Fleischhauer, and S. Diehl, Phys. Rev. X **11**, 021037 (2021).
[28] J. Iles-Smith, N. Lambert, and A. Nazir, Phys. Rev. A **90**, 032114 (2014).
[29] M. Esposito, M. A. Ochoa, and M. Galperin, Phys. Rev. B **92**, 235440 (2015).
[30] A. Bruch, M. Thomas, S. Viola Kusminskiy, F. von Oppen, and A. Nitzan, Phys. Rev. B **93**, 115318 (2016).
[31] M. Carrega, P. Solinas, M. Sassetti, and U. Weiss, Phys. Rev. Lett. **116**, 240403 (2016).
[32] P. Strasberg, G. Schaller, N. Lambert, and T. Brandes, New J. Phys. **18**, 073007 (2016).
[33] D. Newman, F. Mintert, and A. Nazir, Phys. Rev. E **95**, 032139 (2017).
[34] M. Perarnau-Llobet, H. Wilming, A. Riera, R. Gallego, and J. Eisert, Phys. Rev. Lett. **120**, 120602 (2018).
[35] H. J. D. Miller and J. Anders, Nat. Commun. **9**, 2203 (2018).
[36] N. Pancotti, M. Scandi, M. T. Mitchison, and M. Perarnau-Llobet, Phys. Rev. X **10**, 031015 (2020).
[37] A. Rivas, Phys. Rev. Lett. **124**, 160601 (2020).
[38] P. Talkner and P. Hänggi, Rev. Mod. Phys. **92**, 041002 (2020).
[39] M. Popovic, M. T. Mitchison, A. Strathearn, B. W. Lovett, J. Goold, and P. R. Eastham, PRX Quantum **2**, 020338 (2021).
[40] M. Aidelsburger, M. Atala, M. Lohse, J. T. Barreiro, B. Paredes, and I. Bloch, Phys. Rev. Lett. **111**, 185301 (2013).
[41] M. C. Rechtsman, J. M. Zeuner, Y. Plotnik, Y. Lumer, D. Podolsky, F. Dreisow, S. Nolte, M. Segev, and A. Szameit, Nature (London) **496**, 196 (2013).
[42] M. Hafezi, S. Mittal, J. Fan, A. Migdall, and J. M. Taylor, Nat. Photonics **7**, 1001 (2013).
[43] G. Jotzu, M. Messer, R. Desbuquois, M. Lebrat, T. Uehlinger, D. Greif, and T. Esslinger, Nature (London) **515**, 237 (2014).
[44] M. Aidelsburger, M. Lohse, C. Schweizer, M. Atala, J. T. Barreiro, S. Nascimbène, N. R. Cooper, I. Bloch, and N. Goldman, Nat. Phys. **11**, 162 (2015).
[45] B. M. Anderson, R. Ma, C. Owens, D. I. Schuster, and J. Simon, Phys. Rev. X **6**, 041043 (2016).
[46] A. B. Khanikaev and G. Shvets, Nat. Photonics **11**, 763 (2017).
[47] O. Viyuela, A. Rivas, S. Gasparinetti, A. Wallraff, S. Filipp, and M. A. Martin-Delgado, npj Quantum Inf. **4**, 10 (2018).
[48] T. Ozawa, H. M. Price, A. Amo, N. Goldman, M. Hafezi, L. Lu, M. C. Rechtsman, D. Schuster, J. Simon, O. Zilberberg, and I. Carusotto, Rev. Mod. Phys. **91**, 015006 (2019).
[49] T. Chalopin, T. Satoor, A. Evrard, V. Makhalov, J. Dalibard, R. Lopes, and S. Nascimbene, Nat. Phys. **16**, 1017 (2020).
[50] K. Viebahn, J. Minguzzi, K. Sandholzer, A.-S. Walter, M. Sajnani, F. Görg, and T. Esslinger, Phys. Rev. X **11**, 011057 (2021).
[51] F. Ferri, R. Rosa-Medina, F. Finger, N. Dogra, M. Soriente, O. Zilberberg, T. Donner, and T. Esslinger, Phys. Rev. X **11**, 041046 (2021).
[52] See Supplemental Material at http://link.aps.org/supplemental/10.1103/PhysRevLett.128.120403 for the derivation of the exact nonequilibrium steady state, the definitions of the currents, a discussion of particle-hole symmetry, a detailed analysis of the weak-coupling limit and a semiclassical picture for the edge circulation. This includes citations to Refs. [53–56].
[53] C.-K. Chiu, J. C. Y. Teo, A. P. Schnyder, and S. Ryu, Rev. Mod. Phys. **88**, 035005 (2016).
[54] M. B. Plenio and P. L. Knight, Rev. Mod. Phys. **70**, 101 (1998).
[55] V. M. Martinez Alvarez, J. E. Barrios Vargas, M. Berdakin, and L. E. Foa Torres, Eur. Phys. J. Specical Topics **227**, 1295 (2018).
[56] H. M. Price and N. R. Cooper, Phys. Rev. A **85**, 033620 (2012).
[57] A. Dhar, K. Saito, and P. Hänggi, Phys. Rev. E **85**, 011126 (2012).
[58] D. Ryndyk, *Theory of Quantum Transport at Nanoscale* (Springer, Berlin, 2016).
[59] M. T. Mitchison and M. B. Plenio, New J. Phys. **20**, 033005 (2018).
[60] F. D. M. Haldane, Phys. Rev. Lett. **93**, 206602 (2004).
[61] D. Xiao, M.-C. Chang, and Q. Niu, Rev. Mod. Phys. **82**, 1959 (2010).
[62] B. Xing, X. Xu, V. Balachandran, and D. Poletti, Phys. Rev. B **102**, 245433 (2020).